THE JOURNAL OF PHYSICAL CHEMISTRY Letters

PERSPECTIVE

pubs.acs.org/JPCL

Seeing is Believing: Electron Microscopy for Investigating Nanostructures

N. Ravishankar*

Materials Research Centre, Indian Institute of Science, Bangalore 560 012, India

ABSTRACT Controlling the properties of nanostructures requires a detailed understanding of structure, microstructure, and chemistry at ever-decreasing length scales. The modern day transmission electron microscope has thus become an indispensable tool in the study of nanostructures. In this Perspective, we present a brief account of the capabilities of the TEM with some typical examples for characterizing nanostructures. The modern-day TEM has moved from a simple characterization tool to a nanoscale laboratory enabling in situ observation of several fundamental processes at unprecedented resolution levels.

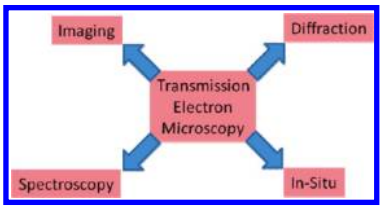

The mention of nanotechnology invariably brings up the much-celebrated talk delivered by Richard Feynman at the 1959 American Physical Society Meeting at Caltech.[1] The talk titled "There Is Plenty of Room at the Bottom" discussed in great detail the problem of manipulating and controlling things at a small scale and is often cited to be the first account of the importance of reducing length scales and the potential of nanotechnology. While talking about the analysis of chemical substances, Feynman pointed out that all that one needed to do was to locate where the atoms were to completely characterize the substance. While the transmission electron microscopes during Feynman's time were not capable of achieving this level of resolution, there has been an immense development in the field today, with modern-day microscopes achieving subangstrom resolution, and thus, we are one step closer to realizing the vision of locating the exact position of atoms. Although the role of the TEM for analyzing biological/beam-sensitive specimens has been debated, there is no doubt that many notable discoveries relating to materials have been enabled by electron microscopy.[2,3] In fact, it is no exaggeration to say that the entire field of nanoscience/technology has gained momentum owing to the imaging capabilities of the modern-day TEM. In this Perspective, we present a brief overview of the underlying principles and the typical capabilities of a modern-day microscope, with particular emphasis on analyzing nanostructures. This account is by no means exhaustive; we have attempted to include typical problems that are associated with analyzing nanostructures and how the modern-day electron microscope may be used to solve these with several examples drawn from our recent work.[4−12]

The mechanism of image formation in transmission electron microscope images is based on the interaction of electrons with matter or, more specifically, how the incident electron interacts with the periodic potential (assuming a crystalline material) of the material under investigation. For the purpose of this Perspective, we adopt a nonrigorous (and often simplified) description of the principles of operation. We refer to the excellent books for details of the technique and the physics of the process.[13−15]

The basic requirement for a TEM sample is that it is electron-transparent. This thickness depends upon the average atomic number of the sample and the incident electron energy; in general, the lower the atomic number or the higher the incident electron energy, the thicker the specimen can be. However, the general rule is that thinner samples are better; samples with a thickness of the order of 100 nm are typically electron-transparent. While the sample preparation step is often the most difficult in the case of bulk materials, nanoparticles are electron-transparent and typically do not require any additional sample preparation. In the conventional TEM mode, a parallel beam of electrons originating from an "electron gun" down the column passes through the specimen and is subsequently viewed/imaged on the screen/camera. The beam, before passing through the specimen, has uniform intensity and travels along a particular direction. The effect of electron scattering by the specimen on the intensity distribution of electrons after passing through the specimen can be understood by considering a situation where there is no sample. In the absence of a sample, the parallel (or nearly parallel) beam simply produces a uniform intensity on the screen below. The presence of a sample in the path of the electron beam has two effects; the spatial uniformity in intensity is changed, and the beam that was unidirectional displays an angular variation in intensity. The spatial variation in intensity after passing through the specimen is called the image, while the angular variation is the diffraction pattern. These two modes constitute the primary modes of operation of a conventional TEM and are illustrated schematically in Figure 1. With the addition of a scanning option, we can also use a fine, converged probe to scan across the sample to

Received Date: February 5, 2010
Accepted Date: March 19, 2010

© XXXX American Chemical Society

DOI: 10.1021/jz100163x | *J. Phys. Chem. Lett.* **2010**, *1*, 1212–1220

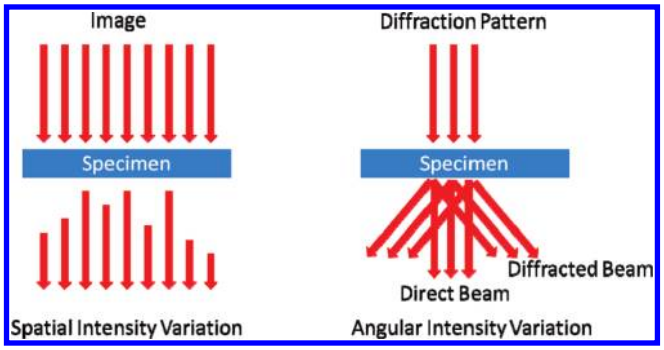

Figure 1. The changes in a uniform, parallel beam of electrons after passing through an electron-transparent specimen. The spatial variation in the intensity of the beam constitutes the image, while the angular variation after passing through the specimen constitutes the diffraction pattern.

obtain either images or diffraction patterns in what is called as the STEM (scanning transmission) mode. The analysis of X-rays generated by the interaction of electrons with the sample provides local chemical information, while the complementary electron energy loss spectroscopy provides spectroscopic fingerprinting of chemistry with local bonding and oxidation state information. Table 1 lists the modes of operation, with typical values of the spatial resolution of each of the above techniques. While there are methods that are superior to TEM in terms of the spatial resolution for imaging (scanning tunneling microscopy STM, for instance) or the energy resolution for spectroscopy (X-ray photoelectron spectroscopy XPS, for instance), the power of the TEM is the combination of imaging, diffraction, and spectroscopy that can be performed on the same small region of the specimen. In this regard, the TEM is unique and unsurpassed and thus has been the most valuable tool for investigating nanostructures.

The spatial variation in intensity after passing through the specimen is called the image, while the angular variation is the diffraction pattern.

Imaging and Diffraction — Real versus Reciprocal Space. The periodicity and the distribution of atoms in crystals can be described in two equivalent mathematical terms. The real space description is based on specifying the coordinates of the atoms in the unit cell that completely describes the structure. An equivalent description is based on the reciprocal lattice, which is a convenient means to describe the phenomenon of diffraction from crystals. Just like the real space comprises a set of lattice points decorated by atoms/group of atoms, the reciprocal space also consists of a set of lattice points, with each point corresponding to a specific set of parallel planes in real space. While imaging enables us to probe the real space, including the distribution of atoms and defects, the diffraction pattern essentially maps the reciprocal space of the crystal. While the interpretation of the features in the reciprocal space may not be as intuitive to interpret as the real space information, the reciprocal space actually contains more useful information/description of the crystal in many cases. In particular, any periodicity in real space is directly reflected in the reciprocal space and is often easier to measure. This periodicity could arise from defects or defect arrays, from composition variations as in spinodal decomposition, or from any other periodic feature in the real space.

While imaging enables us to probe the real space, including the distribution of atoms and defects, the diffraction pattern essentially maps the reciprocal space of the crystal.

Selected-Area Electron Diffraction. The ability to obtain diffraction patterns from small regions in the specimen that can be selected by the user is one of the most powerful features of the TEM. While X-ray diffraction is unmatched in its ability to solve structures with varying levels of complexity, the technique suffers from spatial resolution. For instance, while it is possible to identify the presence of multiple phases using XRD, the spatial distribution of phases and the orientation relationship between the phases cannot be determined directly. In this regard, selected-area electron diffraction is ideally suited to obtain local structural information from areas as small as 0.5 μm, which is limited by the size of the smallest apertures that can be made. In the following section, we present typical examples of electron diffraction patterns from different nanostructures with descriptions of the kind of information that can be obtained in each case.

Figure 2a is an electron diffraction pattern from a cube-shaped particle formed as a result of reduction of $HAuCl_4$ by oleylamine in a toluene medium.[4,16] The pattern can be indexed to a cubic structure, as indicated in the figure. It is interesting to note that the "all odd" rows of reflections (indicated by arrows) have much lower intensities compared to the "all even" reflections, indicating that the cubes possibly have a rocksalt structure with a AuCl stoichiometry.[4] This conclusion is consistent with other observations, including the oxidation state and chemical analysis from the cubes. Thus, while selected-area electron diffraction may not be the best method to solve crystal structures directly, a combination of techniques including SAED can be used to provide valuable information on new structures. A very powerful feature of electron diffraction is the ability to map out the complete reciprocal space by tilting the sample to different low index orientations. With the use of more specialized techniques like convergent-beam electron diffraction, more detailed structural information including space group/point group information can be directly obtained. The smallest area from which diffraction information can be obtained using SAED is limited to about 500 nm. For diffraction information from smaller regions, micro/nanodiffraction techniques can be used,

© XXXX American Chemical Society

DOI: 10.1021/jz100163x | J. Phys. Chem. Lett. 2010, 1, 1212–1220

Table 1. Summary of the Capabilities of Typical Modern-Day Transmission Electron Microscopes with Spatial Resolution

	technique (spatial resolution)	information
imaging	mass thickness contrast (> 1 nm)	distinguishing particles with large difference in average *Z*
	diffraction contrast (~1 nm); bright field/dark field imaging	phases, defects, orientation relationship, growth direction, morphology
	phase contrast (< 0.1 nm); high resolution imaging	atomic structure of defect-free and defect-containing crystals
	Z-contrast (< 0.1 nm); high-angle annular dark field imaging	atomic level distribution of high *Z* elements
diffraction	selected area diffraction (500 nm)	orientation, crystal structure
	microdiffraction/nanobeam diffraction (1−10 nm)	orientation, local structure
	convergent beam electron diffraction (1−10 nm)	point group/space group information
spectroscopy	X-ray energy-dispersive spectroscopy (10 nm)	composition, elemental mapping
	electron energy loss spectroscopy (< 1 nm)	elemental mapping (including light elements),

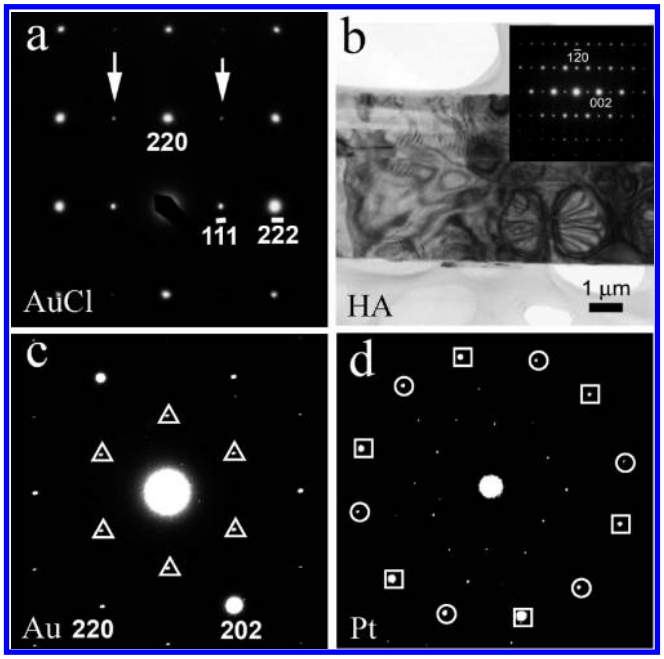

Figure 2. Selected-area diffraction patterns from (a) AuCl cubes, indicating the rocksalt structure (ref 4), (b) from hydroxyapatite platelets, showing the growth direction and the plate orientation (ref 12), (c) from Au platelets, showing the presence of kinematically forbidden 1/3{422} reflections due to the presence of stacking faults (ref 9), and (d) from a Pt platelet with a Σ13 twist boundary formed by rotating two platelets with respect to their common [111] direction by ~28° (ref 9).

where a fine converged probe on the specimen is used to limit the area from which diffraction is obtained. Using this technique, the spatial resolution of electron diffraction can be improved to about 10 nm or less.

Electron diffraction is also extremely useful to determine growth directions and planes in the case of anisotropic nanostructures. For one-dimensional structures like nanorods or wires, electron diffraction patterns can provide direct information on growth directions once the image and the diffraction pattern are oriented properly with respect to each other. In most modern-day microscopes, there is no relative rotation between the image and the diffraction pattern, and the growth direction is easily determined. Figure 2b illustrates the case of a plate-shaped structure of hydroxyapatite grown by wet chemical means.[10,12] The diffraction pattern from the platelet is shown in the inset. The plane normal to the platelet can be determined as the zone axis of the pattern that is shown ([210] in this case), while the growth direction of the platelet obtained by orienting the pattern with respect to the image is found to be [002]. SAED patterns are also extremely useful to determine the orientation relationship between two phases in contact, as has been widely demonstrated in the case of precipitates in metallic alloys.[17]

The fine structure in the diffraction pattern provides vital information on defects present in the structure. For instance, streaking along certain directions in the diffraction pattern indicates the presence of "thin" defects (stacking faults, for instance) perpendicular to the streaking direction. Figure 2c illustrates an example of a diffraction pattern from a Au nanoplatelet which contains stacking faults oriented parallel to the plane of the platelet.[9,10] The presence of such faults, which can be considered to be local hcp slabs in a FCC matrix, leads to the presence of kinematically forbidden 1/3(422) reflections in the [111] zone axis of the FCC structure (marked with triangles). Figure 2d is an illustration of a diffraction pattern from a twist boundary in a Pt platelet.[9] The platelet consists of a twist boundary where one part of the crystal is twisted by ~27° about a common [111] axis. Thus, we see two [111] patterns rotated with respect to each other giving the appearance of a pattern with a nearly 12-fold symmetry. Such composite patterns from multiple phases can be used to determine relative crystal orientations and is extremely valuable for investigating nanoscale heterostructures.

Bright Field, Dark Field, and High Angle Annular Dark Field Imaging. As mentioned earlier, imaging in the TEM refers to the variation in the spatial intensity of the electron beam after interaction with the specimen. The primary mechanism of contrast in the TEM arises from the process of diffraction and is referred to as diffraction contrast. As the incident beam passes through the thin TEM specimen, a dynamic exchange of energy between the direct beam and the diffracted beam takes place as described mathematically by the Howie−Whelan equations. The dynamical theory of diffraction provides a quantitative description of the intensity variation of the direct beam (bright field) and the diffracted beam (dark field) as it passes through the thin specimen and serves as the basis for interpreting contrast from perfect crystals and in crystals containing defects.[15] Figure 3 schematically illustrates the

© XXXX American Chemical Society

DOI: 10.1021/jz100163x | *J. Phys. Chem. Lett.* 2010, *1*, 1212–1220

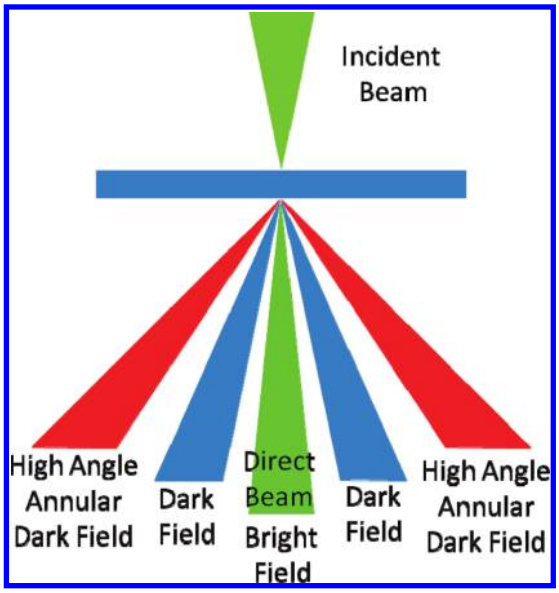

Figure 3. Relative angular relationship between the direct beam used for bright field imaging, diffracted beam used for dark field imaging, and beam scattered to a large angle (typically > 50 mrad) that is used for high-angle annular dark field imaging.

angular spread of the incident beam after it passes through the specimen. Bright field images refer to those formed by selecting the direct beam by introducing an aperture in the back focal plane of the objective lens. The dark regions in a bright field image indicate regions that are favorably oriented for diffraction and as a result of which the intensity in the direct beam is lowered.

Figure 4a is a bright field image of nanoporous Pt clusters formed by controlled aggregation of nanoparticles.[11] The diameter of the clusters is about 60−70 nm, as is evident in this bright field image. The contrast within each cluster indicates the presence of finer-scale features that are not fully resolved here. The first important feature of the clusters is that the mass−thickness contrast is much smaller than that expected from "solid" Pt particles of comparable dimension. This indicates the presence of a significant volume fraction of "voids" in each cluster, indicating the porous nature of the clusters. A dark field image from the same region is shown in Figure 4b. In this case, the aperture in the back focal plane is used to select a portion of the diffracted ring, thus revealing regions in the specimen that diffract to this part of the ring. The bright regions on the order of 2 nm in this image indicate the presence of subunits/grains of this size with each cluster that were not clearly resolved in the bright field image. This indicates that each cluster is built up of subunits on the order of 2 nm that have aggregated to form a porous cluster. Thus, a combination of bright field and dark field images provides a complete description of the morphology and the fine-scale microstructural features in this example.

Scattering to large angles (> 50 mrad) takes place by elastic scattering from atoms with minimal influence from Bragg diffraction. Thus, this scattering intensity is primarily dependent upon the average atomic number of the regions from which the scattering takes place. The use of fine probe and the

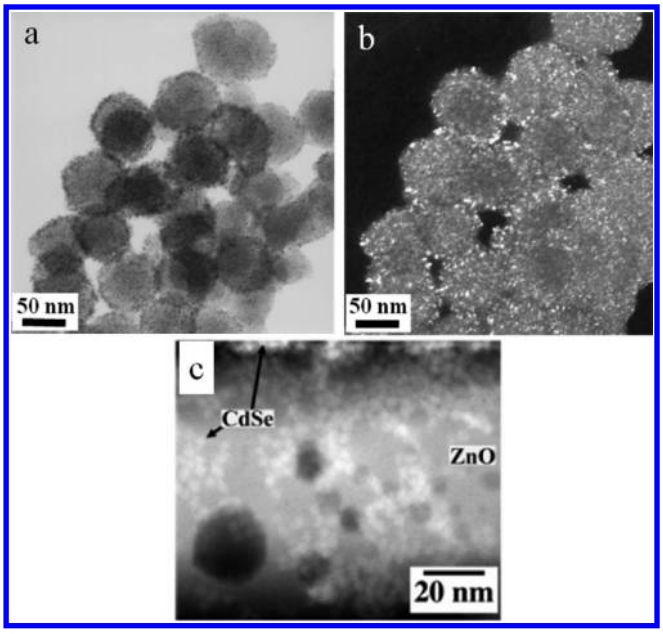

Figure 4. (a) Bright field image of a nanoporous Pt cluster made up of subunits on the order of 2−3 nm and (b) the corresponding dark field image clearly showing the size of the subunits (ref 11). (c) HAADF image showing CdSe quantum dots attached to a ZnO nanostructure (ref 19).

STEM mode enables very high resolution, with the state-of-the-art instruments attaining angstrom-level resolution. For instance, the presence of a single atom of Sb in an atomic column of Si atoms has been demonstrated.[18] Thus, the high-angle annular dark field technique enables atomic-level imaging with *Z*-contrast that is relatively insensitive to defocus, thickness, or specimen orientation. Figure 4c is an illustration of a HAADF image from a sample of ZnO that is sensitized with CdSe quantum dots for solar cell applications.[19] While it is very difficult to image such heterostructures using conventional bright field imaging, the HAADF image clearly shows the brighter regions (appearing as white dots) corresponding to the CdSe dots. HAADF has been successfully employed to analyze core−shell structures of AuPt and has been shown to be a general and powerful technique for the analysis of bimetallic/alloy nanoparticles.[20]

Two of the most common features seen in thin foil specimens arise from variations in the thickness of the foil and effects due to foil bending that are termed thickness fringes and bend contours, respectively.[15] While these are not commonly seen in the case of nanoparticle samples, there are some specific cases where they can be observed. Figure 5a is bright field TEM image of two MgO smoke cubes that have fused along an edge to form a line boundary.[21] While viewed along a [110] direction, the particle consists of two wedges with varying thickness that is manifested in the thickness fringes seen at the edges of the particles and also parallel to the line of contact. Thickness fringes are observed in many other situations and often incorrectly assigned to nonexistent features like composition variations or modulations in the sample. Similarly, bright field images from thin Au platelets (Figure 5b) also show that the presence of bend contours from

© XXXX American Chemical Society

DOI: 10.1021/jz100163x | *J. Phys. Chem. Lett.* **2010**, *1*, 1212–1220

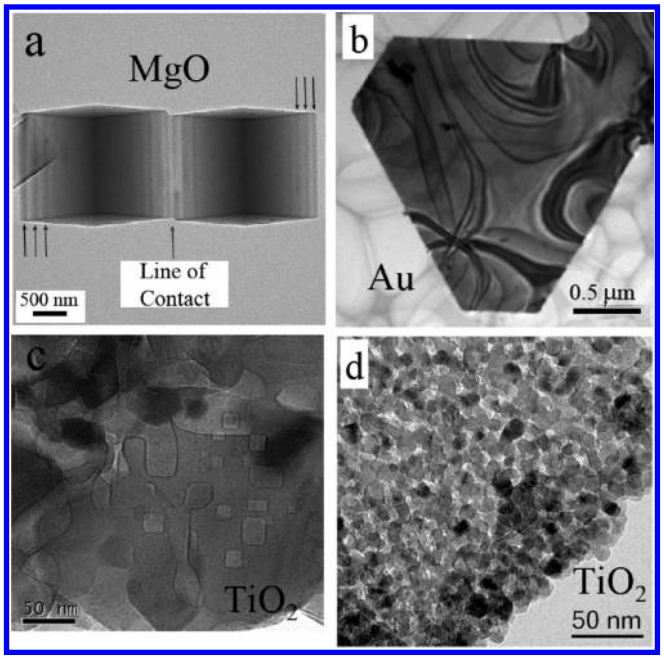

Figure 5. (a) Bright field image of a line boundary between two MgO nanocubes (ref 20). The fringes seen at the edges and the center are due to the thickness variation due to the wedge shape of the specimen. (b) Bend contours in a thin platelet of Au (ref 9). (c) Faceted voids in a large single crystalline region in anatase TiO_2 (ref 6) and (d) nanoporous anatase synthesized by a hybrid sol–gel combustion method (ref 6).

the sense of bending (concave versus convex) can be determined using dark field imaging using different reflections.

Fresnel contrast in TEM images arises in samples containing voids/pores and is seen as a bright/dark fringe around the void depending on whether the image is underfocused or overfocused. Examples of such contrast from a single crystalline TiO_2 sample and a nanoporous TiO_2 sample with internal faceted voids[6] are shown in Figure 5c and d, respectively. The fact that these are internal voids can be confirmed by comparing images at different defocus conditions that show either dark or white fringes in the sample. This is particularly useful when investigating hollow nanoparticles to confirm the existence of internal voids.

Phase Contrast — High-Resolution Imaging. The popularity of the TEM as a characterization technique owes to the ability to produce lattice images of crystalline structures. While the bright field and dark field images represent examples of diffraction contrast, lattice images are phase contrast images typically formed as a result of interference between the direct beam and one or more of the diffracted beams appropriately chosen using an aperture in the back focal plane of the objective lens. The periodicity and symmetry of the interference pattern is dependent upon the spacing and the symmetry of the spots selected in the aperture and represents the underlying lattice. The spots in the diffraction pattern appear even when the crystal is in the off-Bragg condition, and thus, the lattice image is seen even when the crystal planes are not exactly oriented edge-on.

Figure 6a is a high-resolution image from a PbTe crystal oriented along the [001] axis. The (200) and the (020) lattice

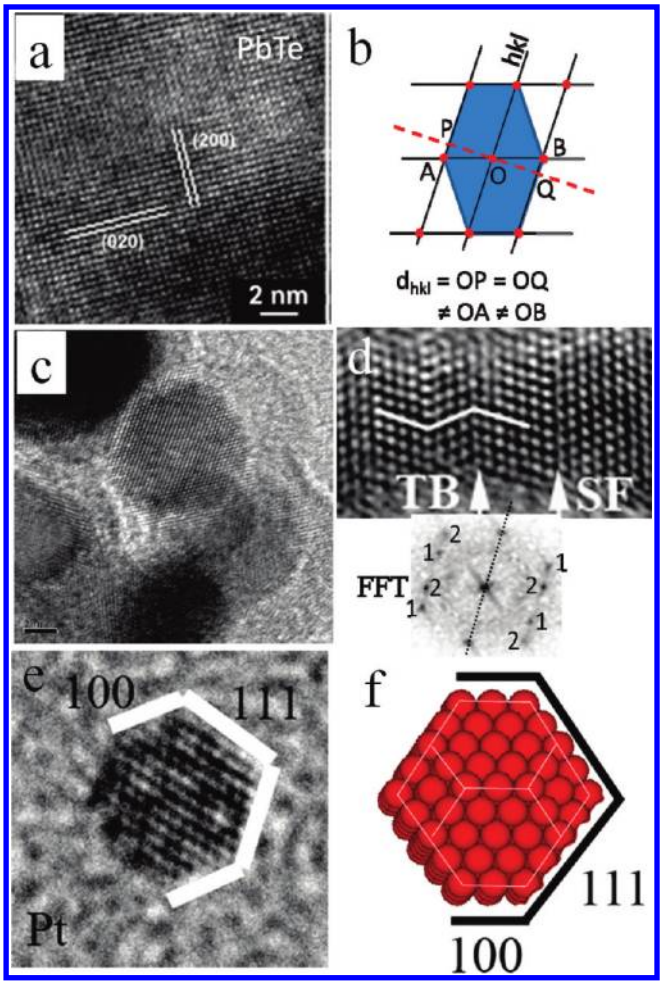

Figure 6. (a) High-resolution image from a PbTe nanorod showing the [200] and [020] planes of the rocksalt structure (ref 7). (b) Schematic illustration of the measurement of lattice spacings from high-resolution images. Measurement along AOB leads to errors in the measurement. (c) Lattice image from a Pt particle in a nanoporous Pt cluster. (d) High-resolution image of defects in a Au nanowire, with the corresponding FFT showing the presence of the twin boundary (ref 5). (e) High-resolution image of ultrafine Pt nanoparticles showing the (100) and the (111) facets. (f) The 3D shape can be reconstructed using a combination of images taken at different orientations.

fringes are seen in this image.[7] The distance between the parallel lines directly gives the interplanar spacing of the corresponding planes. One of the common errors associated with analyzing high-resolution images has to do with obtaining *d* spacings from the lattice images. It is to be noted that the *d* spacings have to be measured as the perpendicular distance between the parallel lattice fringes and not from the spacing between the points. This is analogous to obtaining plane spacing based on the distance between lattice points in the unit cell. While this may be correct in instances where the line connecting the points is perpendicular to the parallel planes, this will lead to wrong values for *d* spacing in all other cases, which is schematically illustrated in Figure 6b. A better method to obtain *d* spacings from high-resolution images is to obtain a fast Fourier transform (FFT) of the desired region of

© XXXX American Chemical Society

DOI: 10.1021/jz100163x | J. Phys. Chem. Lett. 2010, 1, 1212–1220

the images that transforms the sets of parallel lines to spots in the FFT pattern. This transformation provides the mathematical relationship between the real and reciprocal space that was indicated in an earlier section, namely, parallel sets of planes in real space are represented as lattice points in the reciprocal space. Thus, the FFT pattern is a "virtual" diffraction pattern from the two-dimensional "crystal" represented in the lattice image.

High-resolution images are also vital for obtaining detailed understanding of defects in nanostructures. Figure 6c is an example of a high-resolution image of a Pt nanoparticles that is a part of the nanoporous cluster of the type shown in Figure 4a and b. The lattice fringes in this case provide a clear boundary for the nanoparticles and aids in size estimation. Lattice images showing twin defect and stacking faults in a Au nanowire[5] are shown in Figure 6d. The wire is oriented such that the [110] axis is perpendicular to the plane of the paper. The presence of the twin is evident from the FFT of the region containing the twin that clearly shows the presence of a mirror plane. The spots labeled 1 are from one part of the crystal, while the spots labeled 2 are from the twin-related part, clearly showing the mirror symmetry across the dotted line shown in the FFT (Figure 6d). Figure 6e is a high-resolution image from a Pt nanoparticle that is faceted. The FFT from the particle indicates that it is nearly oriented along a [110] direction. In the projected image shown here, the (100) and the (111) facets are seen edge-on, allowing the reconstruction of the 3D shape of the crystal as the expected truncated cuboctahedral shape, as schematically illustrated in Figure 6f.

One of the important problems associated with the analysis of high-resolution images is the so-called delocalization effect that comes about due to the spherical aberration associated with the objective lens. The most important parameter that characterizes the best resolution achievable in TEM is the value of C_s (spherical aberration coefficient) of the objective lens, which is typically on the order of millimeters. The modern-day aberration corrected microscope, with C_s on the order of micrometers, overcomes the problems of image delocalization, and thus, extremely high resolution information can be achieved. Recent studies on multiply twinned nanoparticles have shown that it is possible to obtain a complete mapping of strain in a single particle using an aberration-corrected microscope coupled with image analysis and simulation.[22]

Chemical Mapping in the TEM. There are several methods to obtain compositional information in TEM. In X-ray energy-dispersive analysis (XEDS), the "spectra" is in the form of the intensity of the characteristic X-ray emission, while in electron energy loss spectroscopy (EELS), it is represented as the intensity of energy loss across various ranges of energy. One of the useful ways to couple this information with the underlying microstructural feature is to create chemical maps either in the form of line scans or in the form of 2D images that provide information on the spatial distribution in composition in the sample. XEDS maps in the scanning (STEM) mode or energy-filtered images that are created using specific energy windows characterisitic of specific elements are examples of such maps. Figure 7 is an illustration of a PbSn particle embedded in an Al matrix.[23] The contrast seen in the bright

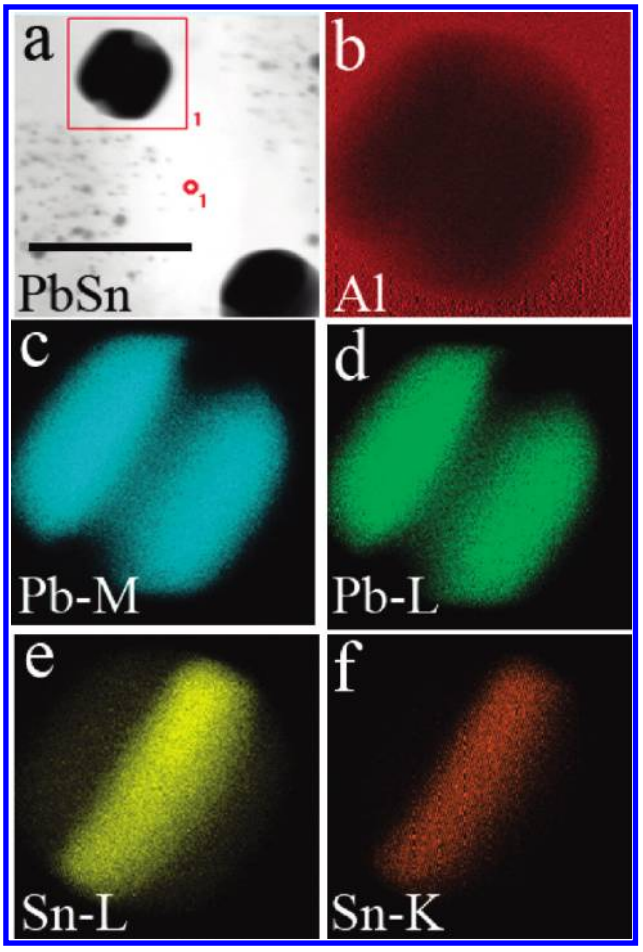

Figure 7. STEM-EDS mapping of composition in a bimetallic nanoparticle (ref 21), showing the distribution of Pb and Sn. (a) Bright field image, b) map using the K X-ray line of Al, (c and d) that using Pb M and L X-ray lines, respectively, and (e and f) that using Sn L and K X-ray lines, respectively. The bar length in (a) corresponds to 500 nm.

field image shown in Figure 7a cannot be unambiguously attributed to chemistry using this image. Figure 7c–f is maps using specific peaks in the spectrum, clearly showing that the contrast in the bright field image is indeed due to differences in chemistry. In this particular example, it clearly reveals the lamellar structure adopted by the PbSn eutectic nanoparticle that is embedded in the matrix. Such maps are extremely useful for delineating phases in the nanoscale.

Figure 8 is an example of EELS spectra obtained along a line from a CeO_2 sample, showing clear differences in the profile from the interior of the particle to the surface. The use of a field emission TEM allows the use of fine probes to obtain the high spatial resolution required for obtaining the line profiles using probes as small as 1.5 nm in diameter.[24] The enrichment of La closer to the surface in the CeO_2 sample is clearly evident from the line profiles that are taken 6 nm apart, as indicated in the high-angle annular dark field images shown. Corresponding changes in the oxidation state of Ce are also observed here, providing a direct correlation between the dopant distribution and local oxidation states in the CeO_2 samples. In addition to being a spectroscopic fingerprinting

© XXXX American Chemical Society

DOI: 10.1021/jz100163x | J. Phys. Chem. Lett. 2010, 1, 1212–1220

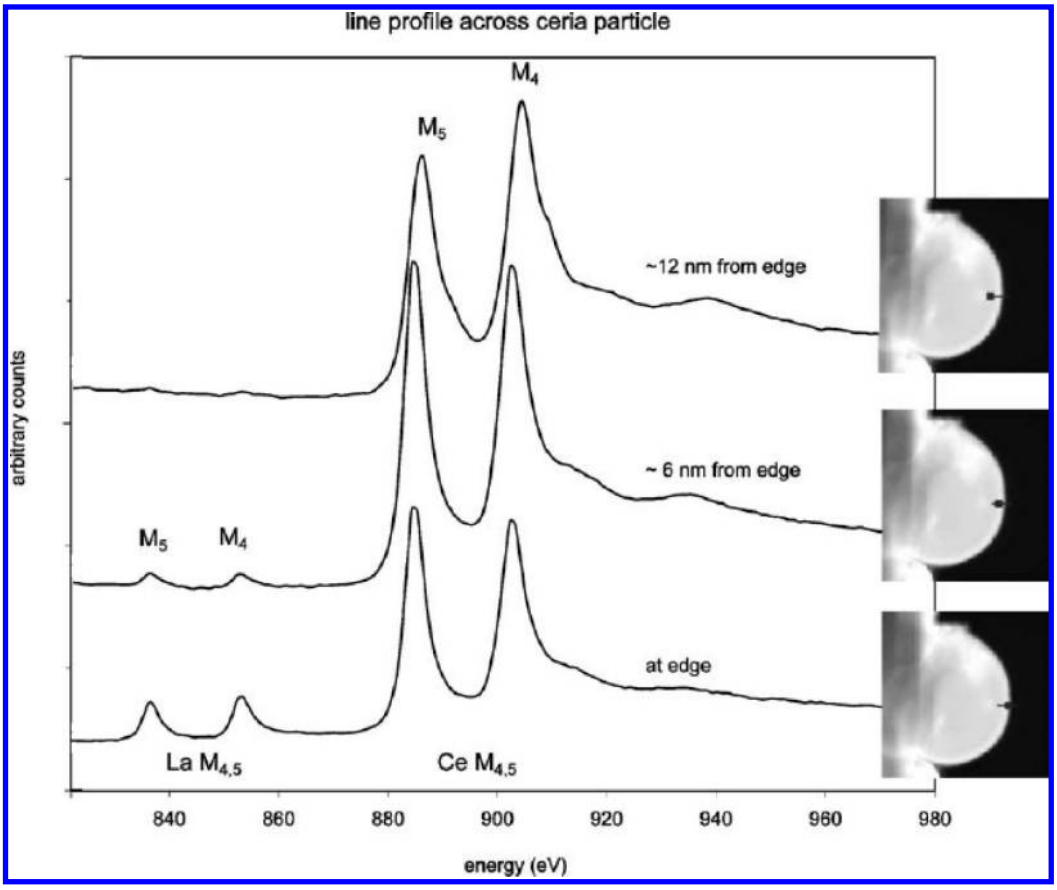

Figure 8. EELS line map along a CeO_2 abrasive particle (ref 22). The three profiles are taken at a distance of 6 nm from each other starting from the interior to the surface of the particle. Clear enrichment of La is seen as we move toward the surface. The corresponding oxidation state change in Ce is also seen here.

technique, EELS has also been successfully employed for imaging surface plasmons in nanostructures. In particular, the enhancement of electric fields due to sharp edges and corners in nanostructures leads to significant enhancement in the localized surface plasmon intensities that can be mapped using EELS in the TEM.[25]

TEM As a Nanoscale Laboratory: In Situ Microscopy. One of the really attractive features of the modern day TEM is the ability to carry out several types of experiments in situ and the ability to record the corresponding changes in the microstructure. While in situ experiments were primarily restricted to heating experiments, the development of specialized holders has dramatically increased the range of experiments to now include in situ scanning microscopy, straining and indentation, reactions under different ambient conditions, crystal growth from the vapor, and even wet chemical reactions.[26−29] An example illustrating the study of melting of embedded Pb nanoparticles in an Al matrix[30] is shown in Figure 9. The sequence of images recorded at different temperatures clearly shows the changes in the morphology of the embedded Pb crystal with increasing temperature. While the particles show clear faceting with slightly rounded edges at lower temperatures, pronounced rounding is observed at temperatures of 350 °C and higher. The perpendicular distance from the center to a particular facet is proportional to the surface/interface energy, and thus, the anisotropy in the interfacial energy is evident at lower temperatures. At higher temperatures, the particles are nearly spherical, indicating that the anisotropy decreases gradually and becomes isotropic when the particle melts.

In summary, the transmission electron microscopy is an indispensible tool for the study of nanostructures, providing microstructural, structural, and chemical information from the same region in the specimen. The possibility of carrying out a variety of in situ experiments truly transforms the TEM into a versatile nanoscale laboratory to obtain fundamental insight into nucleation, growth, and behavior of nanostructures.

The possibility of carrying out a variety of in situ experiments truly transforms the TEM into a versatile nanoscale laboratory to obtain fundamental insight into nucleation, growth, and behavior of nanostructures.

© XXXX American Chemical Society

DOI: 10.1021/jz100163x | *J. Phys. Chem. Lett.* **2010**, *1*, 1212–1220

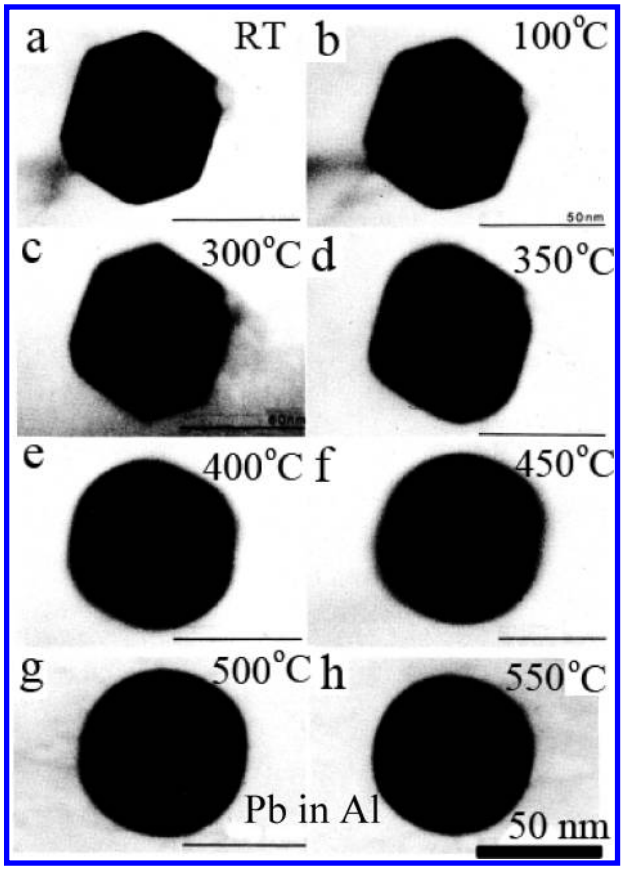

Figure 9. Sequence of images recorded at different temperatures during insitu heating of a sample with Pb particles embedded in an Al matrix, showing clear changes in the faceted morphology of Pb and melting (ref 27).

AUTHOR INFORMATION

Corresponding Author:

Phone: 91-80-2293 3255. Fax: 91-80-2360 7316. E-mail: nravi@mrc.iisc.ernet.in.

Biographies

N. Ravishankar is an Associate Professor at the Materials Research Centre at the Indian Institute of Science. His research interests are centered on understanding the mechanisms of nucleation and growth of nanostructures using TEM as the primary tool. For more information, see http://mrc.iisc.ernet.in/Faculty/Regular/Ravi/Ravi_Profile.htm

ACKNOWLEDGMENT We thank the Nanoscience and Technology Initiative, DST, CSIR, and ISRO for financial assistance.

REFERENCES

(1) Feynman, R. P. There Is Plenty of Room at the Bottom. *Eng. Sci.* **1960,** 22–36.
(2) Segal, M. Surely You're Happy, Mr. Feynman!. *Nat. Nanotechnol.* **2009,** *4*, 786–788.
(3) Toumey, C. Plenty of Room, Plenty of History. *Nat. Nanotechnol.* **2009,** *4*, 783–784.
(4) Halder, A.; Kundu, P.; Ravishankar, N.; Ramanath, G. Directed Synthesis of Rocksalt AuCl Crystals. *J. Phys. Chem. C* **2009,** *113*, 5349–5351.
(5) Halder, A.; Ravishankar, N. Ultrafine Single-Crystalline Gold Nanowire Arrays by Oriented Attachment. *Adv. Mater.* **2007,** *19*, 1854–1858.
(6) Mukherjee, B.; Karthik, C.; Ravishankar, N. Hybrid Sol−Gel Combustion Synthesis of Nanoporous Anatase. *J. Phys. Chem. C* **2009,** *113*, 18204–18211.
(7) Purkayastha, A.; Yan, Q.; Gandhi, D. D.; Li, H.; Pattanaik, G.; Borca-Tasciuc, T.; Ravishankar, N.; Ramanath, G. Sequential Organic−Inorganic Templating and Thermoelectric Properties of High-Aspect-Ratio Single-Crystal Lead Telluride Nanorods. *Chem. Mater.* **2008,** *20*, 4791–4793.
(8) Viswanath, B.; Kundu, P.; Halder, A.; Ravishankar, N. Mechanistic Aspects of Shape Selection and Symmetry Breaking during Nanostructure Growth by Wet Chemical Methods. *J. Phys. Chem. C* **2009,** *113*, 16866–16883.
(9) Viswanath, B.; Kundu, P.; Mukherjee, B.; Ravishankar, N. Predicting The Growth of Two-Dimensional Nanostructures. *Nanotechnology* **2008,** 19.
(10) Viswanath, B.; Kundu, P.; Ravishankar, N. Formation of Two-Dimensional Structures by Tuning the Driving Force of Chemical Reactions: An Interpretation of Kinetic Control. *J. Colloid Interface Sci.* **2009,** *330*, 211–219.
(11) Viswanath, B.; Patra, S.; Munichandraiah, N.; Ravishankar, N. Nanoporous Pt with High Surface Area by Reaction-Limited Aggregation of Nanoparticles. *Langmuir* **2009,** *25*, 3115–3121.
(12) Viswanath, B.; Ravishankar, N. Controlled Synthesis of Plate-Shaped Hydroxyapatite and Implications for the Morphology of the Apatite Phase in Bone. *Biomaterials* **2008,** *29*, 4855–4863.
(13) Edington, J. W. *Practical Electron Microscopy in Materials Science*; Techbooks: Herndon, VA, 1991.
(14) Reimer, L.; Kohl, H. *Transmission Electron Microscopy: Physics of Image Formation*; Springer: New York, 2008.
(15) Williams, D. B.; Carter, C. B. *Transmission Electron Microscopy—A Textbook for Materials Science*; Plenum Press: New York, 1996.
(16) Halder, A.; Ravishankar, N. Gold Nanostructures from Cube-Shaped Crystalline Intermediates. *J. Phys. Chem. B* **2006,** *110*, 6595–6600.
(17) Goswami, R.; Chattopadhyay, K. The Superheating and the Crystallography of Embedded Pb Particles in FCC Al, Cu and Ni Matrices. *Acta Metall. Mater.* **1995,** *43*, 2837–2847.
(18) Voyles, P. M.; Muller, D. A.; Grazul, J. L.; Citrin, P. H.; Gossmann, H.-J. L. Atomic-Scale Imaging of Individual Dopant Atoms and Clusters in Highly N-Type Bulk Si. *Nature* **2002,** *416*, 826–829.
(19) Leschkies, K. S.; Divakar, R.; Basu, J.; Enache-Pommer, E.; Boercker, J. E.; Carter, C. B.; Kortshagen, U. R.; Norris, D. J.; Aydil, E. S. Photosensitization of ZnO Nanowires with CdSe Quantum Dots for Photovoltaic Devices. *Nano Lett.* **2007,** *7*, 1793–1798.
(20) Garcia-Gutierrez, D.; Gutierrez-Wing, C.; Miki-Yoshida, M.; Jose-Yacaman, M. HAADF Study of Au−Pt Core−Shell Bimetallic Nanoparticles. *Appl. Phys. A* **2004,** *79*, 481–87.
(21) Nowak, J. D.; Carter, C. B. Forming Contacts and Grain Boundaries between MgO Nanoparticles. *J. Mater. Sci.* **2009,** *44*, 2408–2418.
(22) Johnson, C. L.; Snoeck, E.; Ezcurdia, M.; Rodriguez-Gonzalez, B.; Pastoriza-Santos, I.; Liz-Marzan, L. M.; Hytch, M. J. Effects of Elastic Anisotropy on Strain Distributions in Decahedral Gold Nanoparticles. *Nat. Mater.* **2008,** *7*, 120–24.

© XXXX American Chemical Society

DOI: 10.1021/jz100163x | *J. Phys. Chem. Lett.* **2010,** *1*, 1212–1220

(23) Bose, S.; Bhattacharya, V.; Chattopadhyay, K.; Ayyub, P. Proximity Effect Controlled Superconducting Behavior of Novel Biphasic Pb−Sn Nanoparticles Embedded in an Al Matrix. *Acta Mater.* **2008,** *56*, 4522–4528.

(24) Gilliss, S. R.; Bentley, J.; Carter, C. B. Electron Energy-Loss Spectroscopic Study of the Surface of Ceria Abrasives. *Appl. Surf. Sci.* **2005,** *241*, 61–67.

(25) Rodriguez-Lorenzo, L.; Alvarez-Puebla, R. A.; Pastoriza-Santos, I.; Stefano, M.; Odile, S.; Mathieu, K.; Liz-Marzan, L. M.; Garcia de Abajo, F. J. Zeptomol Detection through Controlled Ultrasensitive Surface-Enhanced Raman Scattering. *J. Am. Chem. Soc.* **2009,** *131*, 4616–4618.

(26) De Hosson, J. T. M.; Soer, W. A.; Minor, A. M.; Shan, Z.; Stach, E. A.; Syed Asif, S. A.; Warren, O. L. In Situ TEM Nanoindentation and Dislocation-Grain Boundary Interactions: A Tribute to David Brandon. *J. Mater. Sci.* **2006,** *41*, 7704–7719.

(27) Hannon, J. B.; Kodambaka, S.; Ross, F. M.; Tromp, R. M. The Influence of the Surface Migration of Gold on the Growth of Silicon Nanowires. *Nature* **2006,** *440*, 69–71.

(28) Williamson, M. J.; Tromp, R. M.; Vereecken, P. M.; Hull, R.; Ross, F. M. Dynamic Microscopy of Nanoscale Cluster Growth at the Solid−Liquid Interface. *Nat. Mater.* **2003,** *2*, 532–536.

(29) Zheng, H.; Smith, R. K.; Jun, Y.-W.; Kisielowski, C.; Dahmen, U.; Alivisatos, A. P. Observation of Single Colloidal Platinum Nanocrystal Growth Trajectories. *Science* **2009,** *324*, 1309–1312.

(30) Moore, K. I.; Chattopadhyay, K.; Cantor, B. In situ Transmission Electron Microscope Measurements of Solid Al−Solid Pb and Solid Al−Liquid Pb Surface-Energy Anisotropy in Rapidly Solidified Al−5% Pb (by Mass). *Proc. R. Soc. London, Ser. A* **1987,** *414*, 499–507.

© XXXX American Chemical Society

DOI: 10.1021/jz100163x | *J. Phys. Chem. Lett.* **2010,** *1*, 1212–1220